JBC Papers in Press. Published on July 13, 2020 as Manuscript RA120.014901
The latest version is at https://www.jbc.org/cgi/doi/10.1074/jbc.RA120.014901

The role of the I_T-state in D76N β_2-microglobulin amyloid assembly: a crucial intermediate or an innocuous bystander?

Hugh I. Smith[1$], Nicolas Guthertz[1$], Emma E. Cawood[1,2], Roberto Maya-Martinez[1], Alexander L. Breeze[1], Sheena E. Radford[1*]

From the [1]Astbury Centre for Structural Molecular Biology, School of Molecular & Cellular Biology, Faculty of Biological Sciences, University of Leeds, Leeds, LS2 9JT, UK and [2]School of Chemistry, University of Leeds, Leeds LS2 9JT, UK

Running title: The role of the I_T-state in D76N-β_2m aggregation

*To whom correspondence should be addressed: Sheena E. Radford, Astbury Centre for Structural Molecular Biology and School of Molecular and Cellular Biology, University of Leeds, Leeds LS2 9JT Telephone: +44 113 343 3170; email: s.e.radford@leeds.ac.uk.

[$]Equal contribution

Keywords: NMR, CD, β_2-microglobulin, real-time folding, amyloid, D76N, folding intermediate

ABSTRACT

The D76N variant of human β_2-microglobulin (β_2m) is the causative agent of a hereditary amyloid disease. Interestingly, D76N-associated amyloidosis has a distinctive pathology compared with aggregation of wild-type (WT) β_2m which occurs in dialysis-related amyloidosis. A folding intermediate of WT-β_2m, known as the I_T-state, which contains a non-native *trans* Pro32, has been shown to be a key precursor of WT-β_2m aggregation *in vitro*. However, how a single amino acid substitution enhances the rate of aggregation of D76N-β_2m and gives rise to a different amyloid disease remained unclear. Using real-time refolding experiments monitored by CD and NMR, we show that the folding mechanisms of WT- and D76N-β_2m are conserved in that both proteins fold slowly via an I_T-state that has similar structural properties. Surprisingly, however, direct measurement of the equilibrium population of I_T using NMR showed no evidence for an increased population of the I_T-state for D76N-β_2m, ruling out previous models suggesting that this could explain its enhanced aggregation propensity. Producing a kinetically trapped analogue of I_T by deleting the N-terminal six amino acids increases the aggregation rate of WT-β_2m, but slows aggregation of D76N-β_2m, supporting the view that while the folding mechanisms of the two proteins are conserved, their aggregation mechanisms differ. The results exclude the I_T-state as the cause of the rapid aggregation of D76N-β_2m, suggesting that other non-native states must cause its high aggregation rate. The results highlight how a single substitution at a solvent-exposed site can affect the mechanism of aggregation and the resulting disease.

β_2-microglobulin (β_2m) is a component of the major histocompatibility complex class 1 (MHC-1) which plays an important functional role in antigen presentation (1,2). The MHC-1 complex consists of a monomeric heavy chain which is non-covalently assembled with a monomer of β_2m during its biosynthesis in the endoplasmic reticulum (3). Wild-type (WT) human β_2m (WT-β_2m) is a 99 residue, ~12 kDa protein with a seven stranded β-sandwich structure that is stabilised by a single disulfide bond between residues Cys25 and Cys80 (Fig. 1a) (4,5). As part of its normal catabolic cycle WT-β_2m dissociates from the MHC-1 complex, and is cleared from the serum via the kidneys (6). However, in individuals undergoing long-term haemodialysis for kidney failure, WT-β_2m is not cleared effectively from the serum, resulting in an increase in its concentration

from an average of 0.16 μM (five healthy subjects) to 3.2 μM (eleven patients) (6). The increased serum concentration contributes towards the formation of amyloid fibrils which typically deposit in collagen-rich joints, resulting in pathological bone and joint destruction in the disorder known as dialysis-related amyloidosis (6-8).

The folding pathway of WT-β_2m proceeds via a long-lived, structured, folding intermediate known as I_T (9-11). The slow rate of conversion from I_T to the native state (N-state) is caused by the necessary conversion of the peptidyl prolyl bond between His31 and Pro32 from a *trans* to *cis* configuration (11-13). Substitution of Pro32 with natural or non-natural amino acids has shown that the equilibrium population of the I_T-state is directly proportional to the aggregation rate of WT-β_2m (11-15). Consistent with this finding, a truncated form of WT-β_2m in which the N-terminal six residues have been removed, enabling relaxation of Pro32 from *cis* to *trans*, aggregates more rapidly than WT-β_2m, presumably because this variant (known as ΔN6-β_2m) cannot escape the I_T-state (16). ΔN6-β_2m is thus a structural mimic of the I_T-state, and this is supported by the similarity of its ^{1}H-^{15}N-HSQC and far-UV CD spectra with those of the I_T-state populated transiently during real-time refolding experiments (12,16).

In 2012, the first naturally-occurring β_2m variant was identified in a French family as the causative agent of a hereditary, late-onset, fatal and systemic amyloid disease (17). The amyloid fibrils that deposit in the visceral organs of these patients were shown to contain exclusively D76N-β_2m, despite the individuals being heterozygous for the mutation, having normal renal function and normal serum β_2m levels (0.11 – 0.13 μM) (17). Indeed, proteomic analysis of *ex vivo* amyloid fibrils from these patients failed to detect any WT- or ΔN6-β_2m, nor was any truncated D76N-β_2m detected (17). Moreover, no other common amyloid proteins were identified in these deposits by immunohistochemical staining. Most intriguingly, while WT-β_2m does not aggregate *in vitro* at neutral pH, unless additives such as organic solvents, vigorous agitation, collagen or glycosaminoglycans are included (18-20) or the protein is truncated at the N-terminus (creating ΔN6-β_2m) (21), D76N-β_2m aggregates rapidly at neutral pH without the need of these interventions (17).

Various studies have been performed to try to rationalise the difference in the aggregation propensities of WT- and D76N-β_2m. Since the I_T-state is known to be critically important for WT-β_2m aggregation, the folding pathway of D76N-β_2m was investigated by Mangione *et al*. using classical guanidine HCl-induced refolding/unfolding experiments, monitored by tryptophan fluorescence (22). These experiments suggested that D76N-β_2m folds similarly to WT-β_2m, with an initial rapid phase followed by a slow phase corresponding to the *trans* to *cis* isomerisation of Pro32 (22). Based on analysis of the kinetic data, the authors concluded that D76N-β_2m populates the I_T-state to *ca*. 25 % at equilibrium, in marked contrast with its population of only *ca*. 5 % for WT-β_2m, rationalising the increased amyloidogenicity of D76N-β_2m (22). *In silico* studies have also suggested that the I_T-state of D76N-β_2m is structurally distinct to that of WT-β_2m (23,24), raising the possibility that these structural differences may also contribute to the enhanced aggregation propensity of D76N-β_2m. Indeed, one such report suggested that the D76N-β_2m I_T-state has a larger solvent-exposed surface area, a more disordered D-strand and a greater solvation free energy than the WT-β_2m I_T-state, all of which were proposed to contribute to the enhanced aggregation propensity of the protein (23). Alternative models (25) suggest instead that D76N-β_2m forms two different I_T-state structures: the first being the same as the WT-β_2m I_T-state and the second being unique to D76N-β_2m by having unfolded N- and C-terminal regions. Interestingly, the second D76N-β_2m I_T-state was suggested to be more prone to oligomerisation, its formation thus rationalising the rapid aggregation of D76N-β_2m (25).

To cast more light on the reasons for the enhanced amyloidogenicity of D76N-β_2m, and specifically to distinguish between these different models, we analysed the population and structure of the D76N-β_2m I_T-state directly using real-time refolding experiments monitored by far-UV CD and heteronuclear NMR. These experiments provide direct structural and kinetic insights into the intermediate(s) formed during folding (26).

The aggregation propensity of the D76N-β_2m I_T-state was also probed via the generation of an I_T-state structural mimic at equilibrium by truncation of the N-terminal six amino acids of D76N-β_2m (named ΔN6-D76N-β_2m), inspired by the ΔN6-β_2m variant (16). These results revealed that D76N-β_2m folds through an I_T-state that structurally mimics the I_T-state of WT-β_2m. Importantly, direct measurement of the population of the D76N-β_2m I_T-state at equilibrium using NMR revealed that this species is only rarely populated at equilibrium (the I_T-state is below the detection threshold of ^{1}H-^{15}N-HSQC experiments at equilibrium) ruling out models which suggest an enhanced concentration of the I_T-state as the rationale for the increased aggregation kinetics of D76N-β_2m. Instead, we posit that the mutation of Asp to Asn, specifically at position 76 (27), alters the aggregation mechanism of β_2m substantially, such that the rate of aggregation no longer depends on the structure or concentration of the I_T state.

RESULTS

D76N-β_2m folds via an I_T-state that structurally resembles the I_T-state of WT-β_2m

Despite sharing a common immunoglobulin fold and differing only in a single amino acid substitution at a solvent exposed site (Fig. 1a), D76N-β_2m aggregates rapidly at neutral pH, whilst WT-β_2m does not aggregate into amyloid fibrils under the same conditions *in vitro* (Fig. 1b) (17). This raises the possibility that the difference in aggregation behaviour of the two proteins could result from differences in (i) the population of a common amyloidogenic I_T-state, (ii) the structural properties of the I_T-state, or (iii) the proteins' aggregation mechanisms, such that D76N-β_2m does not aggregate via the I_T-state. To distinguish between these possibilities, we examined the conformational properties of the I_T-states of WT- and D76N-β_2m by real-time folding experiments monitored using far-UV CD and compared them with those of ΔN6-β_2m. D76N- and WT-β_2m have essentially identical native protein structures with a root-mean-square deviation (RMSD) of 0.3 Å (Fig. 1a) as well as identical far-UV CD spectra (Supplementary Fig. S1). Despite an RMSD between ΔN6- and WT- or D76N-β_2m of only 1.8 Å and 1.9 Å, respectively (Fig. 1a), the far-UV CD spectrum of ΔN6-β_2m has a larger negative maximum at 216 nm than WT- or D76N-β_2m (Supplementary Fig. S1), presumably resulting from differences in the arrangement of aromatic sidechains in the core of the proteins (14,28). Analysis of the CD spectra of Pro32 variants of β_2m reported similar differences, and showed (assuming a two-state model) that the relative population of the I_T- and N-states at equilibrium can be deduced directly from these spectra (14). Building on these results, WT- and D76N-β_2m were each unfolded at acidic pH (Experimental Procedures). Folding was then initiated by rapidly increasing the pH to 7.4, and far-UV CD spectra were acquired as a function of time until folding was complete (Fig. 2a, b). ΔN6-β_2m, which is trapped at equilibrium in an I_T-like state at pH 7.4, was similarly treated and included for comparison (Fig. 2c). The results showed, as expected (22), that both WT- and D76N-β_2m fold rapidly (in less than a minute) to an I_T-like state, yielding a far-UV CD spectrum with an intense negative maximum at 216 nm that is larger than that of their N-states and typical of that expected for a solution containing a significantly population of the I_T-state (16,22). Subsequent to this transition, slow refolding to the N-state occurs, which involves a decrease in signal intensity in the far-UV CD (Fig. 2a, b). The refolding rate constant for this phase, which maps the I_T- to N-state transition, was 1.03 x 10^{-3} ± 0.03 x 10^{-3} s^{-1} and 1.27 x 10^{-3} ± 0.03 x 10^{-3} s^{-1} for WT- and D76N-β_2m, respectively, indicating that WT- and D76N-β_2m fold to the N-state with similar rates (Fig. 2a, b). Consistent with this interpretation, the slow phase is absent for ΔN6-β_2m as this variant remains trapped in an I_T-like state (Fig. 2c). These experiments confirm previous results which suggested that D76N-β_2m folds slowly to its N-state via an I_T-like species (16,22), and reveal that this species resembles the I_T-state of the WT protein, at least as judged by its far-UV CD spectrum.

To obtain more detailed information about the structural properties of the D76N-β_2m I_T-state, refolding was also monitored in real-time using NMR. We first obtained a full backbone resonance assignment for native D76N-β_2m, as this information was not available in the BMRB (Experimental Procedures). Refolding experiments were initiated by rapidly increasing the pH of the

acid-unfolded proteins to pH 7.4. The first ^{1}H-^{15}N-SOFAST-HMQC spectra of WT- and D76N-β_2m obtained 90 sec after the initiation of refolding show well-dispersed peaks, consistent with the presence of the structured I_T-state which is expected to dominate the refolding reaction at this time point (Fig. 3a and Supplementary Figs. S2 & S4). It is interesting to note that ~14 % and ~13 % of the species populated at this time correspond to native WT- and D76N-β_2m, respectively, as judged by the intensity of resonances unique to the N-state in each spectrum. Importantly, these spectra are distinct from those of the earlier intermediate of WT-β_2m (I_1) and murine β_2m observed previously using non-uniform sampling NMR methods which gives rise to very broad spectra and species shown not to be amyloidogenic (29). As expected, the spectra of the I_T-states of WT- and D76N-β_2m are very similar to one another (Fig. 3a), as well as to spectra previously observed for the WT-β_2m I_T-state (22) and ΔN6-β_2m (16) (obtained under similar conditions, with identical pH and salt concentrations). Using the previously assigned ΔN6-, WT-, and D76N-β_2m spectra in combination, amino acid assignments were transferred to the spectra acquired after a 90 sec refolding time (Supplementary Figs. S2 & S4). 69 peaks were successfully assigned for WT-β_2m and 58 for D76N-β_2m, allowing the chemical shifts of resonances in the I_T-states of WT- and D76N-β_2m to be compared (Fig. 3b). This showed that significant chemical shift perturbations (CSPs) are observed only for residues in the EF-loop (residues 71 to 78, which contains the D76N substitution) and the structurally adjacent AB-loop (residues 12 to 20) (Fig. 1a and Fig. 3b). The ^{1}H-^{15}N-SOFAST-HMQC spectra of native (N-state) WT- and D76N-β_2m (obtained after a folding time of 180 min (Supplementary Figs. S3 & S4) are also similar, with the only significant chemical shift differences again involving residues in the AB- and EF-loops (Fig. 3d). The similar CSPs between WT- and D76N-β_2m at 90 sec (I_T-state) and 180 min (N-state) refolding times (Fig. 3b, d) show that the folding of both proteins involves a kinetically long-lived I_T-state that has similar structural properties for both β_2m variants, at least as judged by these approaches.

The β_2m folding energy landscape is unperturbed by the D76N substitution

Given the similarities in the folding mechanisms of WT- and D76N-β_2m, the remarkable difference in their rates of aggregation into amyloid could result from differences in the population of the I_T-state at equilibrium, which would be reflected by differences in the rate of folding/unfolding of I_T-state to/from the N-state. Indeed, such a scenario was posited previously based on analysis of their folding kinetics using tryptophan fluorescence (22). Consistent with this view, the population of the I_T-state in WT-β_2m variants (such as P32G-, P5G- and ΔN6-β_2m) have been shown to correlate with their aggregation rates (14). The rate of the I_T- to N-state transition of WT- and D76N-β_2m was investigated at the single residue level by fitting the ^{1}H-^{15}N-SOFAST-HMQC peak volumes for resonances which have a unique chemical shift in their N-states (i.e. they do not overlap with peaks arising from I_T-state). For WT-β_2m/D76N-β_2m 70/66 peaks could be identified as unique to their N-states (Supplementary Figs. S3 & S5). The intensity of these peaks was monitored as a function of the refolding time and fitted to a single exponential function (Experimental Procedures) (Fig. 4a-d), from which 40/37 per-residue refolding rate constants, respectively, could be determined with confidence (Fig. 4e, f). Of note is that the peak volume is not zero in the initial spectrum obtained after 90 sec, reflecting a small population (<15%) of molecules that fold rapidly to the N-state presumably since they represent the small population of molecules with a *cis* Pro32 in the unfolded state (Fig. 4a-d). The data revealed that the I_T- to N-state transition proceeds at a similar rate for all residues monitored for WT- and D76N-β_2m, with median rate constants of 0.62 x 10^{-3} ± 0.05 x 10^{-3} s^{-1} and 0.63 x 10^{-3} ± 0.04 x 10^{-3} s^{-1}, respectively. Hence the energy barrier for the I_T- to N-state transition is similar for both proteins.

A similar kinetic analysis was carried out focusing on peaks which are unique to the I_T-state, (i.e. they do not overlap with peaks rising from N-state) (Supplementary Fig. S6). In the spectra obtained after a 90 sec refolding time, 26/25 peaks are unique to the I_T-states for WT-β_2m/D76N-β_2m, respectively (Supplementary Figs. S2 & S4). The intensity of these peaks was also monitored as a

function of the refolding time and fitted to a single exponential (Experimental Procedures) (Supplementary Fig. S6a-d), from which 20/19 per-residue refolding rate constants for WT- and D76N-β_2m, respectively, could be determined with confidence (Supplementary Fig. S6e, f). This analysis also showed similar kinetic behaviour for WT- and D76N-β_2m, with the decrease in intensity of I_T-state peaks occurring with median rate constants of 0.56 x 10^{-3} s^{-1} ± 0.06 x 10^{-3} s^{-1} and 0.49 x 10^{-3} ± 0.05 x 10^{-3} s^{-1}, respectively (Supplementary Fig. S6e, f). The similarity in rate constants for different residues throughout the protein sequence for these transitions provides strong evidence in support of a two-state I_T- to N-state transition. In addition, the results show that the energy barrier between the I_T-state and the N-state is essentially unperturbed by the D76N substitution.

The unique chemical shifts for residues in the I_T- and N-states also enable the equilibrium populations of the I_T- and N-states in WT- and D76N-β_2m to be directly determined using NMR. Previous results have shown that the population of the I_T-state is less than 5 % for WT-β_2m at equilibrium under the conditions used (22). Consistent with this, despite contouring into the noise of the native WT-β_2m spectrum, resonances unique to the I_T-state could not be observed. The lowest contour level of this spectrum is 12-fold below that of the other spectra shown (Fig. 5a). Despite high signal-to-noise of these spectra, no evidence for resonances which are unique to the I_T-state of WT-β_2m could be observed in the noise of its N-state spectrum (see for example resonances for Ser11 and Ser52 in Fig. 5a), implying a low equilibrium population of the I_T-state. Importantly, the lack of detectable I_T-state resonances in the spectrum of native D76N-β_2m (Fig. 5b) demonstrates a similar low equilibrium population of I_T-state for this protein, consistent with the similarities of these variants' far-UV CD spectra presented in Supplementary Fig. S1. Thus, the D76N-β_2m I_T-state has similar structure, relative population and interconversion rates with the N-state as the WT-β_2m I_T-state, providing clear evidence that the amyloidogenicity of D76N-β_2m cannot be attributed to differences in the I_T-state.

Generation of a kinetically-trapped D76N-β_2m I_T-state mimic

In order to determine the aggregation propensity of the D76N-β_2m I_T-state directly, a truncated product of the D76N-β_2m variant was produced in which the N-terminal six residues were removed, inspired by previous findings that ΔN6-β_2m mimics the I_T-state of WT-β_2m (16,29,30), referred to as ΔN6-D76N-β_2m (Experimental Procedures). As anticipated, the ^{1}H-^{15}N-SOFAST-HMQC spectrum of this variant closely resembles the spectrum of the D76N-β_2m I_T-state captured transiently during refolding, indicating that ΔN6-D76N-β_2m is indeed an I_T-state mimic of D76N-β_2m (Fig. 6a). Interestingly, measurement of the rate of aggregation of the different proteins into amyloid fibrils using ThT fluorescence showed that ΔN6-D76N-β_2m is *less* aggregation-prone than its full-length counterpart, by contrast with truncation of the N-terminal six residues from WT-β_2m which dramatically *increases* the rate of its aggregation (compare Fig. 1b and Fig. 6b). Fitting the normalised ThT fluorescence intensity data yielded aggregation half-time (T_{half}) values of 24.7 ± 9.5 h for ΔN6-D76N-β_2m, 18.0 ± 1.9 h for ΔN6-β_2m and 6.6 ± 0.7 h for D76N-β_2m (Table 1). Hence, of these three variants, D76N-β_2m aggregates most rapidly despite containing a *cis* Pro32 and an intact N-terminal sequence.

Finally, the effect of deleting the N-terminal six residues on the stability of D76N-β_2m was measured using temperature denaturation monitored by far-UV CD (Fig. 6c). The results revealed an apparent midpoint temperature ($T_{m,app}$) of denaturation (Table 1) with the rank order of stability ΔN6-D76N-β_2m < D76N-β_2m ~ ΔN6-β_2m < WT-β_2m. The results demonstrate that the T_{half} aggregation does not correlate with thermodynamic stability. Interestingly, the results also showed that the difference in $T_{m,app}$ between ΔN6- and WT-β_2m is 10.3 °C, a value similar to that obtained by deletion of the N-terminal six residues in D76N-β_2m (11.8 °C) (Table 1). Thus, there is little cross-talk between the N-terminal hexapeptide and the effect of the amino acid substitution at position 76 on protein stability.

DISCUSSION

The native-like folding intermediate of WT-β_2m, known as the I_T-state, is central to the mechanism of its assembly into amyloid (14,31). Here, we have examined in detail the contribution of the I_T-state to the aggregation mechanism of the closely-related D76N-β_2m variant, building on previous results which suggested that the population and/or structural properties of this state could rationalise the dramatically enhanced ability of the protein to aggregate into amyloid both *in vitro* and *in vivo* (22). The slow folding rate of WT- and D76N-β_2m was exploited here to enable direct analysis of the I_T- to N-state transition using real-time far-UV CD and NMR spectroscopy. The results revealed that D76N-β_2m folds via an I_T-state which structurally resembles the WT-β_2m I_T-state. Analysis of the refolding kinetics in residue-specific detail showed that the activation barrier between the I_T- and N-states in WT- and D76N-β_2m is similar. This implies a similar degree of destabilisation of the I_T-state, transition state and N-state by the substitution of Asp to Asn at position 76 (in agreement with all species having native-like structural properties). Moreover, the relative populations of the I_T- and N-state at equilibrium are also not perturbed by the D76N substitution. Hence, by contrast with previous reports (22), our evidence shows that the enhanced amyloidogenicity of D76N-β_2m cannot be explained by increased population of I_T-state or by any substantial differences in its structural properties (although subtle differences in conformation not reflected in $^1H/^{15}N$ chemical shifts cannot be ruled out). Finally, the decreased stability of D76N-β_2m relative to the WT protein does not explain its increased amyloid potential, since other β_2m variants with similar or even further reduced stability compared with D76N-β_2m, including murine-β_2m (29), V37A-β_2m (32) and the ΔN6-D76N-β_2m variant described here, all aggregate more slowly than D76N-β_2m.

The similarity of the WT- and D76N-β_2m I_T-states is further suggested by the similarity in the aggregation rates of ΔN6- and ΔN6-D76N-β_2m, both of which are presumably trapped in an I_T-like state. Strikingly, this rate is slower than that of the parent D76N-β_2m variant, demonstrating that while the D76N-β_2m I_T-state is aggregation-prone, its formation cannot be rate-determining for aggregation of the full-length protein. This suggests that D76N-β_2m aggregates by a mechanism distinct from that of its WT counterpart for which the I_T-state population determines the rate of aggregation. Instead aggregation of D76N-β_2m could be initiated by formation of a different non-native, but structured species, possibly the previously identified N*-state observed in D76N-β_2m crystals (33). Alternatively, aggregation may occur from more highly disordered state(s) of the protein, with the D76N substitution increasing the amyloidogenicity of these species by altering their conformational properties. Such a mechanism has been posited for immunoglobulin light chains associated with light chain amyloidosis based on the orientation of the two β-strands linked by the disulfide bond in the native monomer and in the amyloid fold (34). In addition, the role of flanking regions in tailoring amyloidogenicity has been observed in several other proteins that aggregated from a disordered state, including α-synuclein (35) and tau (36). A different aggregation pathway and precursor species in D76N-β_2m could also explain the subtle differences in the WT- and D76N-β_2m fibril secondary structures determined using solid state NMR and/or cryo-electron microscopy (EM) (33,37-40).

In summary, the results presented here demonstrate that the mechanisms of aggregation of WT- and D76N-β_2m differ significantly, with the WT protein aggregating via formation of the I_T-state, while for D76N-β_2m a different native-like-state (N*-state) (33) or perhaps a more highly unfolded state (41) could be rate-determining for aggregation. These differences in mechanism, involving different precursor(s), may also explain the radical differences between the systemic amyloidosis caused by D76N-β_2m and the pathology of dialysis-related amyloidosis caused by the WT protein. Indeed, at normal serum concentrations, D76N-β_2m aggregates into amyloid without involvement of the WT protein in these heterozygous individuals (22). By contrast, for WT-β_2m aggregation involves truncation of the N-terminus to form ΔN6-β_2m, the isomerisation of *cis* Pro32 to *trans* (29,30), and the involvement of collagen, glycosaminoglycans and other extracellular factors to create amyloid that deposits specifically in the joints (18,32,42,43). Our results thus highlight the fundamental difference in the *in*

vitro aggregation mechanism and the consequences in diseases brought by a single amino acid substitution in a solvent-exposed loop of a protein with a simple 99-residue immunoglobulin fold.

EXPERIMENTAL PROCEDURES

Protein expression and purification

^{14}N-, ^{15}N-, and ^{15}N-^{13}C-labelled proteins were expressed and purified as described previously (30). D76N-ΔN6-β_2m was particularly prone to precipitation when resuspending the lyophilised material during purification, and so care was taken to ensure that resuspension was always carried out in 20 mM sodium phosphate, pH 7.4. All proteins were purified in the last step using gel filtration and care was taken to only collect the centre of the monomer peak so as to exclude the possibility of oligomers in the preparations. Analysis using SEC-MALLS, native ESI-MS and by re-injecting the protein onto the column after concentration did not reveal the detectable presence of oligomers in the preparations.

Real-time refolding monitored by far-UV CD

Proteins (30 μM) were dialysed against the unfolding solution (0.8 M urea, 25 mM sodium phosphate buffer at pH 2.5) for 1 h. To initiate refolding, the unfolded proteins were rapidly diluted with 300 mM sodium phosphate buffer, pH 7.4 (2:1 (*v/v*) unfolded protein:refolding buffer) at 20 °C. Data acquisition was initiated immediately after addition of the refolding buffer into the CD cuvette which already contained the unfolded protein (dead-time ~ 1 sec). Spectra (200-260 nm) were acquired using a ChirascanTM plus CD spectrometer (Applied Photophysics). One spectrum was recorded per min, using a step size of 1 nm and a sampling time of 0.5 sec per point.

Real-time refolding monitored using NMR

Protein samples (450 μM) were dialysed against the unfolding solution (1.5 M urea, 25 mM sodium phosphate buffer at pH 2.5 containing 10 % (*v/v*) D_2O) for 1 h. To initiate refolding, 150 μl of refolding buffer (500 mM sodium phosphate, pH 7.4) was added to 350 μl of each unfolded protein (final protein concentration 300 μM in 167 mM sodium phosphate buffer, pH 7.4). These experiments were carried out at 20 °C. The sample was immediately added to the NMR tube and data acquisition was initiated (dead-time ~ 30 sec). The folding reaction was monitored by acquiring ^{1}H-^{15}N-SOFAST-HMQC (44) spectra every 60 sec, with 100 points in f1 (^{15}N) and 956 in f2 (^{1}H), and two scans were acquired per increment. Spectra were recorded on a 600 MHz Bruker AVANCE III HD spectrometer equipped with a 5mm QCI-P (proton-observe inverse quadruple resonance) cryoprobe, using spectral widths of 15.97 ppm in f2 and 22.00 ppm in f1.

Spectra were processed in NMRPipe (45) and analysed with the software package PINT (46). Peak volumes were determined by fitting to a Lorentzian line shape. The total peak volume of each residue was plotted as a function of time and fitted to a single exponential to determine the refolding rate constant:

$$y = -ae^{-bx} + c \qquad \textbf{Equation 1}$$

or

$$y = ae^{-bx} + c \qquad \textbf{Equation 2}$$

where y is the intensity of the chosen peak at time x, c is the value of y at infinite time, a is the initial intensity and b is the rate constant. For positive peaks, Equation 1 was used to fit peaks unique to the N-state and Equation 2 was used to fit peaks unique to the I_T-state.

Chemical shift perturbations (CSPs) were calculated using Equation 3:

$$CSP = \sqrt{\left(5\delta\ ^{1}H\right)^2 + \left(\delta^{15}N\right)^2} \qquad \textbf{Equation 3}$$

where $\delta\ ^{1}H$ and $\delta^{15}N$ are the differences in the ^{1}H and ^{15}N chemical shifts for the two resonances being compared.

Thermal denaturation monitored by far-UV CD

For thermal denaturation experiments an initial spectrum of the sample (20 μM protein in 25 mM sodium phosphate buffer, pH 7.4), was obtained at 25 °C. The temperature of the solution was decreased to 20 °C, and then increased in 5 °C steps with an equilibration time of 120 sec at each temperature, up to a final temperature of 90 °C. At the end of the temperature ramp, the sample was cooled to 25 °C and a spectrum acquired to determine if the transition was reversible. Each spectrum was acquired from 190 nm to 260 nm

with a step size of 1 nm and 1 sec per point sampling. Two spectra were acquired for each temperature and averaged. The path length used was 1 mm. The data were fitted to a two-state equilibrium (Equation 4) using the software package CDPal (47).

$$E = e^{-\frac{\Delta H_m}{R}\left(\frac{1}{T_m}-\frac{1}{T}\right)-\frac{\Delta C_p}{R}\left(\frac{T_m}{T}-1+\ln\left(\frac{T}{T_m}\right)\right)} \quad \textbf{Equation 4}$$

where ΔH_m is the change in enthalpy at the denaturation midpoint T_m, ΔC_p is the difference in heat capacity between the two states, R is the gas constant and T the temperature (Kelvin). ΔC_p was assumed to be independent of temperature. Since the thermal denaturation process was not fully reversible, $T_{m,ap}$ values are quoted.

***In vitro* fibrillation assays**

Protein samples (stored either as lyophilised powder and resolubilised immediately before used in 25 mM sodium phosphate buffer pH 7.4, or as concentrated solution at -80 °C) were centrifuged at 14000 x g for 10 min, the supernatant was filtered (0.22 μm, Millipore), diluting the same as appropriate to give a final protein concentration of 30 μM in 25 mM sodium phosphate pH 6.2, 137 mM NaCl, 10 μM ThT, 0.02 % (*w/v*) NaN_3. Each protein (ten replicates, 100 μl each) was added to Corning 96 well polystyrene microtiter plates, sealed with clear polyolefin film (STARLAB) and incubated at 37 °C for at least 48 h with constant shaking at 600 rotations per minute (rpm). ThT fluorescence was monitored (excitation 440 nm and emission 480 nm) with a Fluostar Optima, BMG Labtech plate reader.

T_{half} values were calculated by fitting normalised data (between 0 to 1) for each replicate to Equation 5, and determining the time taken to reach half the maximal intensity:

$$Y(t) = A + \frac{K-A}{\left(1+Qe^{-B(t-M)\frac{1}{v}}\right)} \quad \textbf{Equation 5}$$

where A is the pre-transition baseline (lower asymptote), K is the post-transition baseline (upper asymptote), B is the growth rate and M is the time of maximal growth. Q and v are parameters which affect the transitions from and to the growth phase, Y is the normalised signal and t is time (48,49).

Negative stain transmission EM

Carbon coated copper EM grids were placed coated-side down onto sample drops containing undiluted material from the *in vitro* fibrillation assay for 30 sec. The grids were then blotted with filter paper to remove excess solvent and sample. Grids were then placed onto drops of 2 % (*w/v*) uranyl acetate for 30 sec, blotted again and air-dried. Images were taken using a Jeol 1400 microscope using a 120 keV Lab6 filament and Gatan US1000XP 2k x 2k CCD camera.

D76N-β$_2$m NMR assignment

The assignment of D76N-β_2m was performed in 25 mM sodium phosphate, 83 mM sodium chloride at pH 7.4 and 25 °C. ^{15}N and ^{15}C uniformly labelled protein was used to acquire all NMR experiments needed to accomplish the backbone and side chains assignment. Triple resonance HNCO, HNCA, HN(co)CA, HN(co)CACB, (h)CCH-TOCSY, H(c)CH-TOCSY NMR experiments were recorded on a Bruker AVANCE III HD 750 MHz spectrometer equipped with triple resonance inverse cryoprobe. Spectra were processed using NMRPipe and analysed using CcpNmr Analysis (version 2.4) (50).

^{1}H, ^{15}N and ^{13}C chemical shifts were deposited in the Biological Magnetic Resonance Data Bank (BMRB) (deposition number 50302).

Data Availability

All raw data from the results presented will be made available upon request: please contact Sheena Radford (**s.e.radford@leeds.ac.uk**). ^{1}H, ^{15}N and ^{13}C chemical shift assignments for D76N are available at BRMB (accession number 50302).

Acknowledgments

We thank members of our laboratories for helpful discussions and Nasir Khan for his excellent technical support. We acknowledge funding from the Wellcome Trust (105222/Z/14/Z (Hugh Smith), 109984 (Nicolas Guthertz) and 109154 (Emma Cawood)). We are also grateful to the University of Leeds and the Wellcome Trust (094232) for funding for the Chiroscan CD spectrometer and for access to the Astbury Biostructure Laboratory EM and BioNMR Facilities.

Conflict of interest

The authors declare that they have no conflicts of interest with the contents of this article.

References

1. Cresswell, P., Ackerman, A. L., Giodini, A., Peaper, D. R., and Wearsch, P. A. (2005) Mechanisms of MHC class I-restricted antigen processing and cross-presentation. *Immunol Rev* **207**, 145-157
2. Germain, R. N. (1986) The ins and outs of antigen processing and presentation. *Nature* **322**, 687-689
3. Campbell, E. C., Antoniou, A. N., and Powis, S. J. (2012) The multi-faceted nature of HLA class I dimer molecules. *Immunology* **136**, 380-384
4. Smith, D. P., and Radford, S. E. (2001) Role of the single disulphide bond of beta(2)-microglobulin in amyloidosis in vitro. *Protein Sci* **10**, 1775-1784
5. Isenman, D. E., Painter, R. H., and Dorrington, K. J. (1975) The structure and function of immunoglobulin domains: studies with beta-2-microglobulin on the role of the intrachain disulfide bond. *Proc Natl Acad Sci U S A* **72**, 548-552
6. Floege, J., Bartsch, A., Schulze, M., Shaldon, S., Koch, K. M., and Smeby, L. C. (1991) Clearance and synthesis rates of beta 2-microglobulin in patients undergoing hemodialysis and in normal subjects. *J Lab Clin Med* **118**, 153-165
7. Kay, J. (1999) Beta 2-microglobulin amyloidosis in renal failure: understanding this recently recognized condition. *Cleve Clin J Med* **66**, 145-147
8. Otsubo, S., Kimata, N., Okutsu, I., Oshikawa, K., Ueda, S., Sugimoto, H., Mitobe, M., Uchida, K., Otsubo, K., Nitta, K., and Akiba, T. (2009) Characteristics of dialysis-related amyloidosis in patients on haemodialysis therapy for more than 30 years. *Nephrol Dial Transplant* **24**, 1593-1598
9. Chiti, F., Mangione, P., Andreola, A., Giorgetti, S., Stefani, M., Dobson, C. M., Bellotti, V., and Taddei, N. (2001) Detection of two partially structured species in the folding process of the amyloidogenic protein beta 2-microglobulin. *J Mol Biol* **307**, 379-391
10. Chiti, F., De Lorenzi, E., Grossi, S., Mangione, P., Giorgetti, S., Caccialanza, G., Dobson, C. M., Merlini, G., Ramponi, G., and Bellotti, V. (2001) A partially structured species of beta 2-microglobulin is significantly populated under physiological conditions and involved in fibrillogenesis. *J Biol Chem* **276**, 46714-46721
11. Jahn, T. R., Parker, M. J., Homans, S. W., and Radford, S. E. (2006) Amyloid formation under physiological conditions proceeds via a native-like folding intermediate. *Nat Struct Mol Biol* **13**, 195-201
12. Kameda, A., Hoshino, M., Higurashi, T., Takahashi, S., Naiki, H., and Goto, Y. (2005) Nuclear magnetic resonance characterization of the refolding intermediate of beta2-microglobulin trapped by non-native prolyl peptide bond. *J Mol Biol* **348**, 383-397
13. Sakata, M., Chatani, E., Kameda, A., Sakurai, K., Naiki, H., and Goto, Y. (2008) Kinetic coupling of folding and prolyl isomerization of beta2-microglobulin studied by mutational analysis. *J Mol Biol* **382**, 1242-1255
14. Eichner, T., and Radford, S. E. (2009) A generic mechanism of beta2-microglobulin amyloid assembly at neutral pH involving a specific proline switch. *J Mol Biol* **386**, 1312-1326
15. Torbeev, V., Ebert, M. O., Dolenc, J., and Hilvert, D. (2015) Substitution of proline32 by alpha-methylproline preorganizes beta2-microglobulin for oligomerization but not for aggregation into amyloids. *J Am Chem Soc* **137**, 2524-2535

16. Eichner, T., Kalverda, A. P., Thompson, G. S., Homans, S. W., and Radford, S. E. (2011) Conformational conversion during amyloid formation at atomic resolution. *Mol Cell* **41**, 161-172
17. Valleix, S., Gillmore, J. D., Bridoux, F., Mangione, P. P., Dogan, A., Nedelec, B., Boimard, M., Touchard, G., Goujon, J. M., Lacombe, C., Lozeron, P., Adams, D., Lacroix, C., Maisonobe, T., Plante-Bordeneuve, V., Vrana, J. A., Theis, J. D., Giorgetti, S., Porcari, R., Ricagno, S., Bolognesi, M., Stoppini, M., Delpech, M., Pepys, M. B., Hawkins, P. N., and Bellotti, V. (2012) Hereditary systemic amyloidosis due to Asp76Asn variant beta2-microglobulin. *N Engl J Med* **366**, 2276-2283
18. Benseny-Cases, N., Karamanos, T. K., Hoop, C. L., Baum, J., and Radford, S. E. (2019) Extracellular matrix components modulate different stages in beta2-microglobulin amyloid formation. *J Biol Chem* **294**, 9392-9401
19. Ohhashi, Y., Kihara, M., Naiki, H., and Goto, Y. (2005) Ultrasonication-induced amyloid fibril formation of beta2-microglobulin. *J Biol Chem* **280**, 32843-32848
20. Yamamoto, S., Yamaguchi, I., Hasegawa, K., Tsutsumi, S., Goto, Y., Gejyo, F., and Naiki, H. (2004) Glycosaminoglycans enhance the trifluoroethanol-induced extension of beta 2-microglobulin-related amyloid fibrils at a neutral pH. *J Am Soc Nephrol* **15**, 126-133
21. Esposito, G., Michelutti, R., Verdone, G., Viglino, P., Hernandez, H., Robinson, C. V., Amoresano, A., Dal Piaz, F., Monti, M., Pucci, P., Mangione, P., Stoppini, M., Merlini, G., Ferri, G., and Bellotti, V. (2000) Removal of the N-terminal hexapeptide from human beta2-microglobulin facilitates protein aggregation and fibril formation. *Protein Sci* **9**, 831-845
22. Mangione, P. P., Esposito, G., Relini, A., Raimondi, S., Porcari, R., Giorgetti, S., Corazza, A., Fogolari, F., Penco, A., Goto, Y., Lee, Y. H., Yagi, H., Cecconi, C., Naqvi, M. M., Gillmore, J. D., Hawkins, P. N., Chiti, F., Rolandi, R., Taylor, G. W., Pepys, M. B., Stoppini, M., and Bellotti, V. (2013) Structure, folding dynamics, and amyloidogenesis of D76N beta2-microglobulin: roles of shear flow, hydrophobic surfaces, and alpha-crystallin. *J Biol Chem* **288**, 30917-30930
23. Chong, S. H., Hong, J., Lim, S., Cho, S., Lee, J., and Ham, S. (2015) Structural and thermodynamic characteristics of amyloidogenic intermediates of beta-2 microglobulin. *Sci Rep* **5**, 13631
24. Loureiro, R. J. S., Vila-Vicosa, D., Machuqueiro, M., Shakhnovich, E. I., and Faisca, P. F. N. (2017) A tale of two tails: The importance of unstructured termini in the aggregation pathway of beta2-microglobulin. *Proteins* **85**, 2045-2057
25. Loureiro, J. S. R., Vila-Vicosa, D., Machuqueiro, M., Shakhnovich, E. I., and Faisca, F. N. P. (2019) The early phase of beta-2 microglobulin aggregation: an integrative computational study framed on the D76N mutant and the DeltaN6 variant. *Biomolecules* **9**, 366
26. Zhuravleva, A., and Korzhnev, D. M. (2017) Protein folding by NMR. *Prog Nucl Magn Reson Spectrosc* **100**, 52-77
27. de Rosa, M., Barbiroli, A., Giorgetti, S., Mangione, P. P., Bolognesi, M., and Ricagno, S. (2015) Decoding the structural bases of D76N beta2-microglobulin high amyloidogenicity through crystallography and asn-scan mutagenesis. *PLoS One* **10**, e0144061

28. Calabrese, M. F., Eakin, C. M., Wang, J. M., and Miranker, A. D. (2008) A regulatable switch mediates self-association in an immunoglobulin fold. *Nat Struct Mol Biol* **15**, 965-971
29. Karamanos, T. K., Pashley, C. L., Kalverda, A. P., Thompson, G. S., Mayzel, M., Orekhov, V. Y., and Radford, S. E. (2016) A population shift between sparsely populated folding intermediates fetermines amyloidogenicity. *J Am Chem Soc* **138**, 6271-6280
30. Karamanos, T. K., Jackson, M. P., Calabrese, A. N., Goodchild, S. C., Cawood, E. E., Thompson, G. S., Kalverda, A. P., Hewitt, E. W., and Radford, S. E. (2019) Structural mapping of oligomeric intermediates in an amyloid assembly pathway. *Elife* **8**, 46574
31. Eichner, T., and Radford, S. E. (2011) Understanding the complex mechanisms of beta2-microglobulin amyloid assembly. *FEBS J* **278**, 3868-3883
32. Myers, S. L., Jones, S., Jahn, T. R., Morten, I. J., Tennent, G. A., Hewitt, E. W., and Radford, S. E. (2006) A systematic study of the effect of physiological factors on beta2-microglobulin amyloid formation at neutral pH. *Biochemistry* **45**, 2311-2321
33. Le Marchand, T., de Rosa, M., Salvi, N., Sala, B. M., Andreas, L. B., Barbet-Massin, E., Sormanni, P., Barbiroli, A., Porcari, R., Sousa Mota, C., de Sanctis, D., Bolognesi, M., Emsley, L., Bellotti, V., Blackledge, M., Camilloni, C., Pintacuda, G., and Ricagno, S. (2018) Conformational dynamics in crystals reveal the molecular bases for D76N beta-2 microglobulin aggregation propensity. *Nat Commun* **9**, 1658
34. Radamaker, L., Lin, Y. H., Annamalai, K., Huhn, S., Hegenbart, U., Schonland, S. O., Fritz, G., Schmidt, M., and Fandrich, M. (2019) Cryo-EM structure of a light chain-derived amyloid fibril from a patient with systemic AL amyloidosis. *Nat Commun* **10**, 1103
35. Doherty, C. P. A., Ulamec, S. M., Maya-Martinez, R., Good, S. C., Makepeace, J., Khan, G. N., van Oosten-Hawle, P., Radford, S. E., and Brockwell, D. J. (2020) A short motif in the N-terminal region of alpha-synuclein is critical for both aggregation and function. *Nat Struct Mol Biol* **27**, 249-259
36. Chen, D., Drombosky, K. W., Hou, Z., Sari, L., Kashmer, O. M., Ryder, B. D., Perez, V. A., Woodard, D. R., Lin, M. M., Diamond, M. I., and Joachimiak, L. A. (2019) Tau local structure shields an amyloid-forming motif and controls aggregation propensity. *Nat Commun* **10**, 2493
37. Barbet-Massin, E., Ricagno, S., Lewandowski, J. R., Giorgetti, S., Bellotti, V., Bolognesi, M., Emsley, L., and Pintacuda, G. (2010) Fibrillar vs crystalline full-length beta-2-microglobulin studied by high-resolution solid-state NMR spectroscopy. *J Am Chem Soc* **132**, 5556-5557
38. Debelouchina, G. T., Platt, G. W., Bayro, M. J., Radford, S. E., and Griffin, R. G. (2010) Magic angle spinning NMR analysis of beta2-microglobulin amyloid fibrils in two distinct morphologies. *J Am Chem Soc* **132**, 10414-10423
39. Iadanza, M. G., Silvers, R., Boardman, J., Smith, H. I., Karamanos, T. K., Debelouchina, G. T., Su, Y., Griffin, R. G., Ranson, N. A., and Radford, S. E. (2018) The structure of a beta2-microglobulin fibril suggests a molecular basis for its amyloid polymorphism. *Nat Commun* **9**, 4517
40. Su, Y., Sarell, C. J., Eddy, M. T., Debelouchina, G. T., Andreas, L. B., Pashley, C. L., Radford, S. E., and Griffin, R. G. (2014) Secondary structure in the core of amyloid

fibrils formed from human beta-2 microglobulin and its truncated variant DeltaN6. *J Am Chem Soc* **136**, 6313-6325
41. Visconti, L., Malagrino, F., Broggini, L., De Luca, C. M. G., Moda, F., Gianni, S., Ricagno, S., and Toto, A. (2019) Investigating the molecular basis of the aggregation propensity of the pathological D76N mutant of beta-2 microglobulin: role of the denatured state. *Int J Mol Sci* **20**, 396
42. Stoppini, M., and Bellotti, V. (2015) Systemic amyloidosis: lessons from beta2-microglobulin. *J Biol Chem* **290**, 9951-9958
43. Relini, A., Canale, C., De Stefano, S., Rolandi, R., Giorgetti, S., Stoppini, M., Rossi, A., Fogolari, F., Corazza, A., Esposito, G., Gliozzi, A., and Bellotti, V. (2006) Collagen plays an active role in the aggregation of beta2-microglobulin under physiopathological conditions of dialysis-related amyloidosis. *J Biol Chem* **281**, 16521-16529
44. Schanda, P., and Brutscher, B. (2005) Very fast two-dimensional NMR spectroscopy for real-time investigation of dynamic events in proteins on the time scale of seconds. *J Am Chem Soc* **127**, 8014-8015
45. Delaglio, F., Grzesiek, S., Vuister, G. W., Zhu, G., Pfeifer, J., and Bax, A. (1995) NMRPipe: a multidimensional spectral processing system based on UNIX pipes. *J Biomol NMR* **6**, 277-293
46. Ahlner, A., Carlsson, M., Jonsson, B. H., and Lundstrom, P. (2013) PINT: a software for integration of peak volumes and extraction of relaxation rates. *J Biomol NMR* **56**, 191-202
47. Niklasson, M., Andresen, C., Helander, S., Roth, M. G., Zimdahl Kahlin, A., Lindqvist Appell, M., Martensson, L. G., and Lundstrom, P. (2015) Robust and convenient analysis of protein thermal and chemical stability. *Protein Sci* **24**, 2055-2062
48. Cohen, S. I., Vendruscolo, M., Dobson, C. M., and Knowles, T. P. (2012) From macroscopic measurements to microscopic mechanisms of protein aggregation. *J Mol Biol* **421**, 160-171
49. Arosio, P., Knowles, T. P., and Linse, S. (2015) On the lag phase in amyloid fibril formation. *Phys Chem Chem Phys* **17**, 7606-7618
50. Vranken, W. F., Boucher, W., Stevens, T. J., Fogh, R. H., Pajon, A., Llinas, M., Ulrich, E. L., Markley, J. L., Ionides, J., and Laue, E. D. (2005) The CCPN data model for NMR spectroscopy: development of a software pipeline. *Proteins* **59**, 687-696
51. Trinh, C. H., Smith, D. P., Kalverda, A. P., Phillips, S. E., and Radford, S. E. (2002) Crystal structure of monomeric human beta-2-microglobulin reveals clues to its amyloidogenic properties. *Proc Natl Acad Sci U S A* **99**, 9771-9776

Footnotes

The abbreviations used are: **β_2m**, β_2-microglobulin; **ThT**, Thioflavin T; **MHC-I**, Major Histocompatibility Complex Class I; **EM**, Electron Microscopy; **Ig**, Immunoglobulin; **WT**, Wild-Type; **I_T**, native-like folding Intermediate; **N**, Native; **T_{half}**, half-Time; **$T_{m,app}$**, apparent midpoint Temperature; **rpm**, rotation per minute; **MD**, Molecular Dynamics; **CSPs**, Chemical Shift Perturbations; **w/v**, weight/volume; **RMSD**, root-mean-square deviation; **v/v**, volume/volume

Figures and Figure Legends

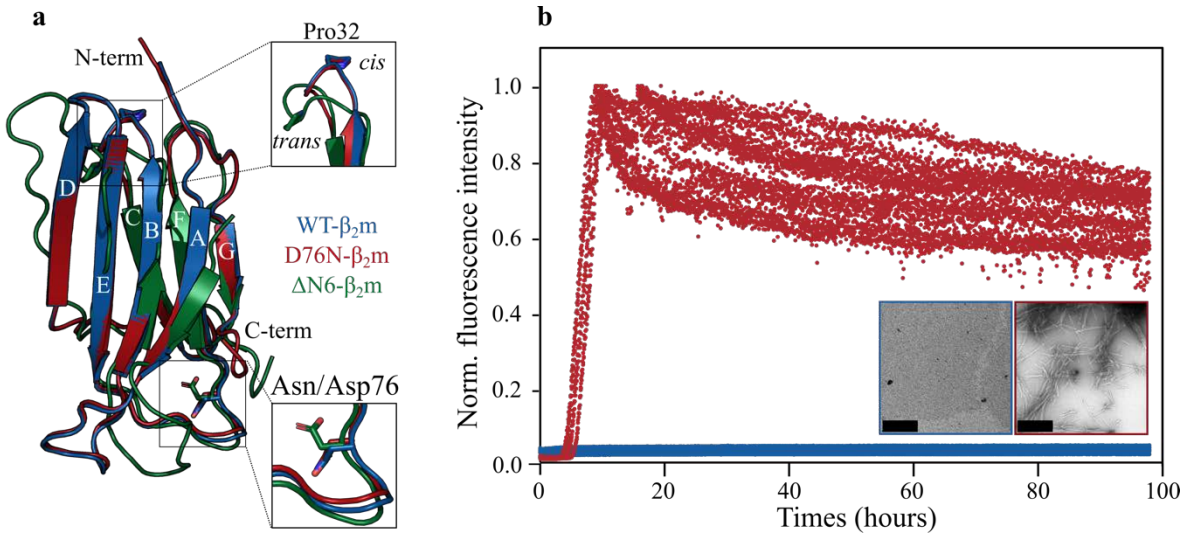

Figure 1. Structure and amyloidogenicity of WT-, D76N- and ΔN6-β₂m.
(a) Superposition of the crystal structures of WT- (blue; PDB: 1LDS (51)) and D76N-β_2m (red; PDB: 4FXL (17)), and the lowest-energy structure of ΔN6-β_2m determined using NMR (green; PDB: 2XKU (16)). The insets highlight the BC loop, which contains Pro32, and the EF loop, which contains residue 76. **(b)** Aggregation kinetics of WT- and D76N-β_2m (coloured as (a)) measured using thioflavin T (ThT) fluorescence. Experiments were performed with 30 μM protein in 25 mM sodium phosphate pH 6.2, 137 mM NaCl, 10 μM ThT, 0.02 % (*w/v*) NaN_3, at 37 °C, 600 rpm. 10 replicates are shown. Negative stain transmission electron microscopy images of the assay endpoints (taken after 100 h) are shown as insets, framed in the same colours. The scale bar corresponds to 300 nm.

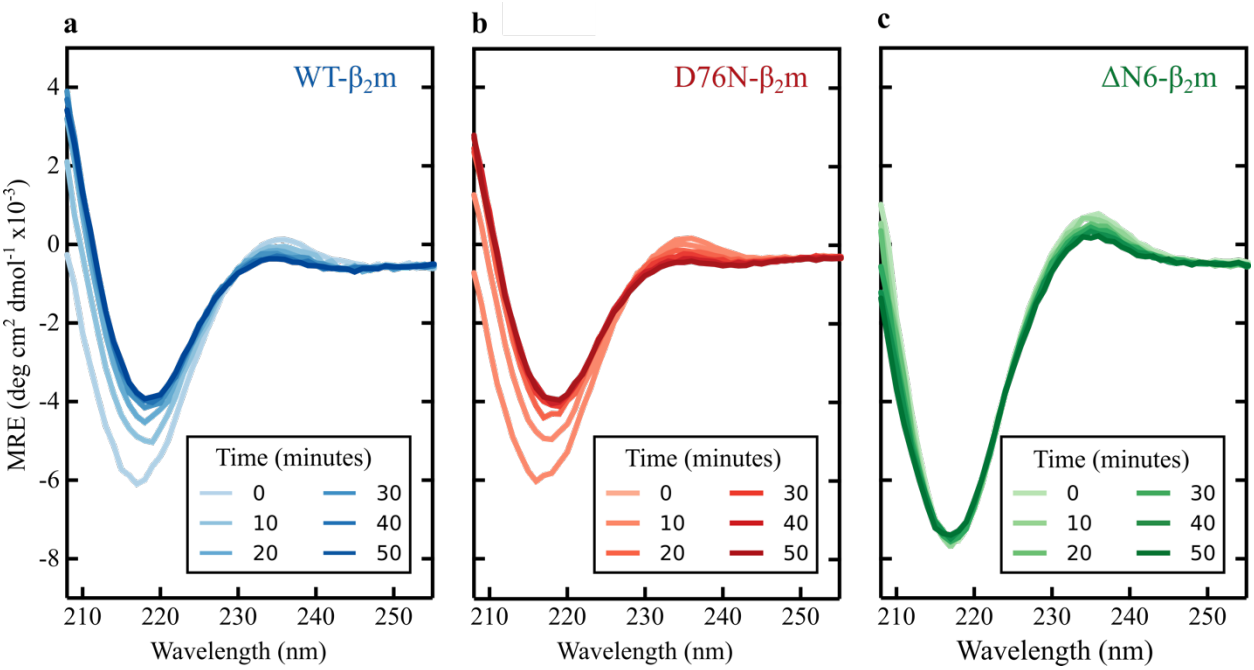

Figure 2. Real-time refolding of WT-, D76N- and ΔN6-β_2m, monitored by far-UV CD.
WT-β_2m is in blue **(a)**, D76N-β_2m is in red **(b)** and ΔN6-β_2m is in green **(c)**. Spectra were recorded every minute over the refolding time-course, however only spectra acquired at 10 min intervals are shown here for clarity. In all plots, spectra are shaded darker as the time-course progresses. These experiments were carried out at 20 °C at a final protein concentration of 20 μM in 100 mM sodium phosphate buffer, pH 7.4. MRE corresponds to the molar ellipticity.

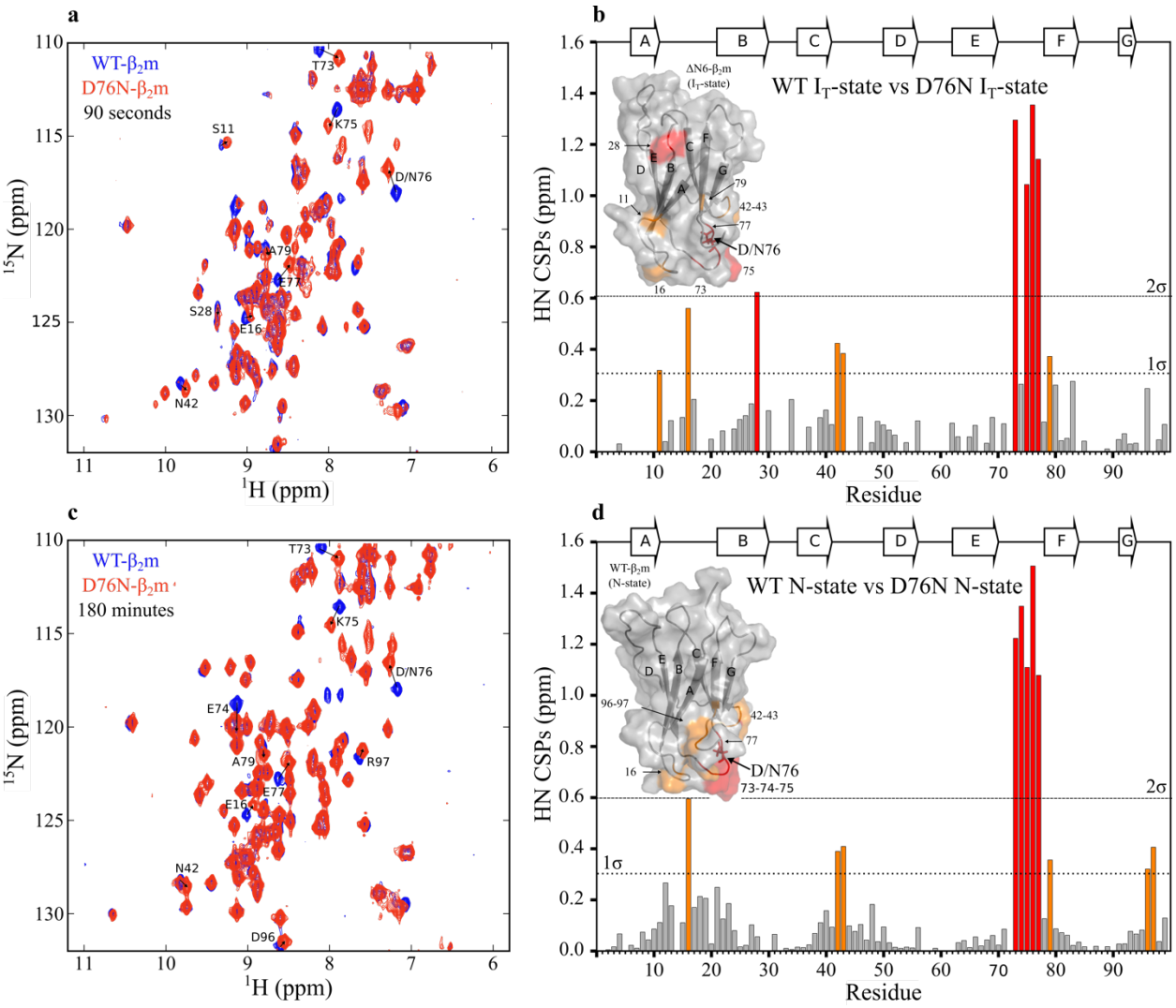

Figure 3. Real-time refolding of WT- and D76N-β$_2$m, monitored by ^{1}H-^{15}N NMR spectroscopy. **(a)** ^{1}H-^{15}N-SOFAST-HMQC spectra for WT- (blue) and D76N-β$_2$m (red) recorded 90 sec after the initiation of refolding by pH jump (Experimental Procedures). Assignments of the 90 sec spectra (I_T-state) are shown in Supplementary Figs. S2 & S4 for WT- and D76N-β$_2$m, respectively. **(b)** CSPs between spectra of WT- and D76N-β$_2$m shown in (a). The CSP was calculated for the 58 peaks successfully assigned for the I_T-state of both WT- and D76N-β$_2$m (Supplementary Figs. S2 & S4, respectively). **(c)** ^{1}H-^{15}N-SOFAST-HMQC spectra of WT- (blue) and D76N-β$_2$m (red) recorded 180 min after the initiation of refolding. **(d)** CSPs between spectra of WT- and D76N-β$_2$m shown in (c). The CSP was calculated for the 87 peaks successfully assigned for the N-states of both WT- and D76N-β$_2$m (Supplementary Figs. S3 & S5, respectively). (a, c) Only positive contours are shown. ^{1}H-^{15}N resonances for Gly18 and Gly43 are therefore not present in this figure as they have negative intensities due to folding of the spectrum in the ^{15}N dimension. Residues with significant chemical shift differences are labelled. (b, d) CSPs <1σ (dotted line) from the mean of all CSPs are coloured in grey; those between 1σ and 2σ are coloured orange and > 2σ from the mean are coloured red. CSPs are mapped onto the solution structures of ΔN6- (PDB: 2XKU (16)) or WT-β$_2$m (PDB: 2XKS (16)) for (b) and (d), respectively, using the same colour code. These experiments were carried out at 20 °C at a final protein concentration of 300 μM in 1.0 M urea and 167 mM sodium phosphate buffer, pH 7.4.

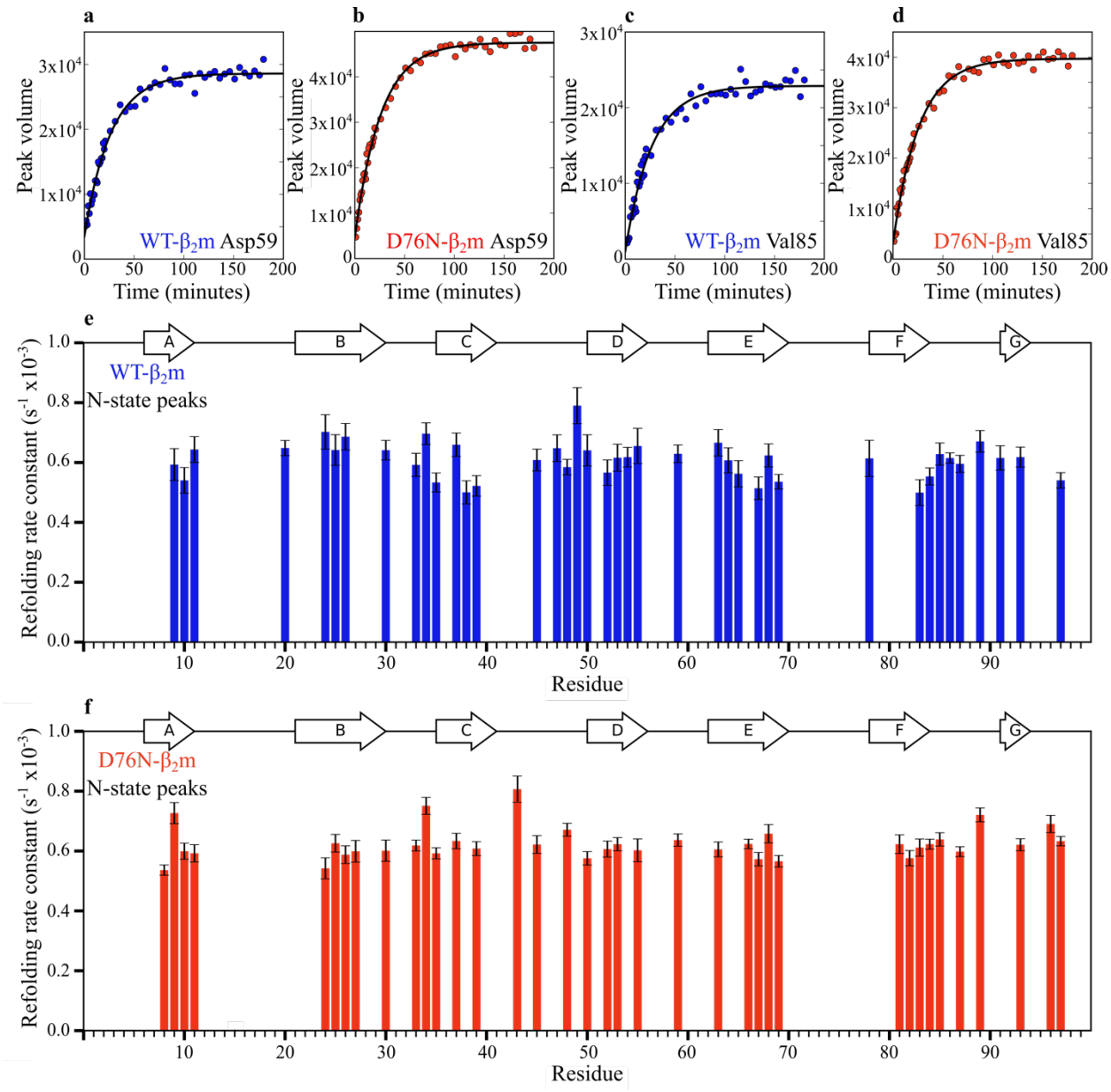

Figure 4. Single-residue refolding rates for N-state peaks of WT- and D76N-β₂m, monitored by NMR spectroscopy.

(a-d) Representative data and fits in black for single residue folding rates fitted with Equation 1 (Experimental Procedures). **(e, f)** The rate constants for individual residues that could be measured with confidence (where the error on the fit is no more than 3 median absolute deviations of all errors within each dataset) are shown in (e) and (f) for WT- and D76N-β₂m, respectively. Error bars are the fitting errors.

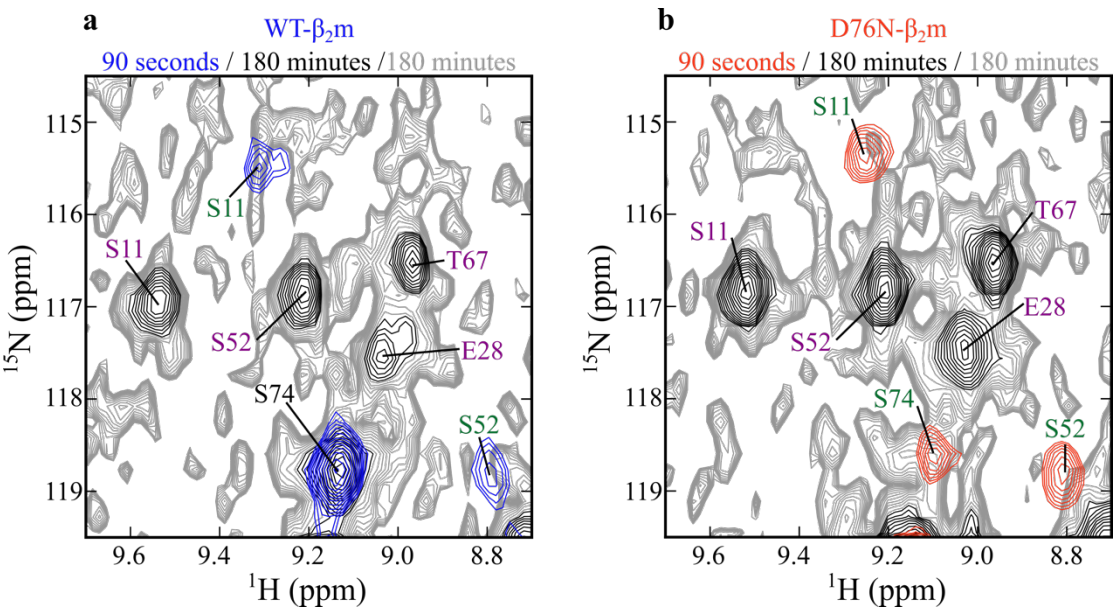

Figure 5. Searching for I_T-state peaks in the N-state ^{1}H-^{15}N-SOFAST-HMQC spectra of native WT- and D76N-β_2m.

The spectra of WT- **(a)** and D76N-β_2m **(b)** taken at 180 min (black contours) after refolding are compared with the corresponding spectra taken at 90 sec (blue contours for WT-β_2m and red contours for D76N-β_2m). The native protein spectra obtained after a refolding time of 180 min are contoured to show the spectral noise (grey) down to a level 12-fold below that of the lowest black contour. The peaks unique to the I_T-state are labelled in green, those unique to the N-state are labelled in purple and peaks common between the I_T-state and the N-state are labelled in black. There is no evidence of observable resonances from the I_T-state in the spectra of the native proteins, consistent with a very low population of I_T at equilibrium.

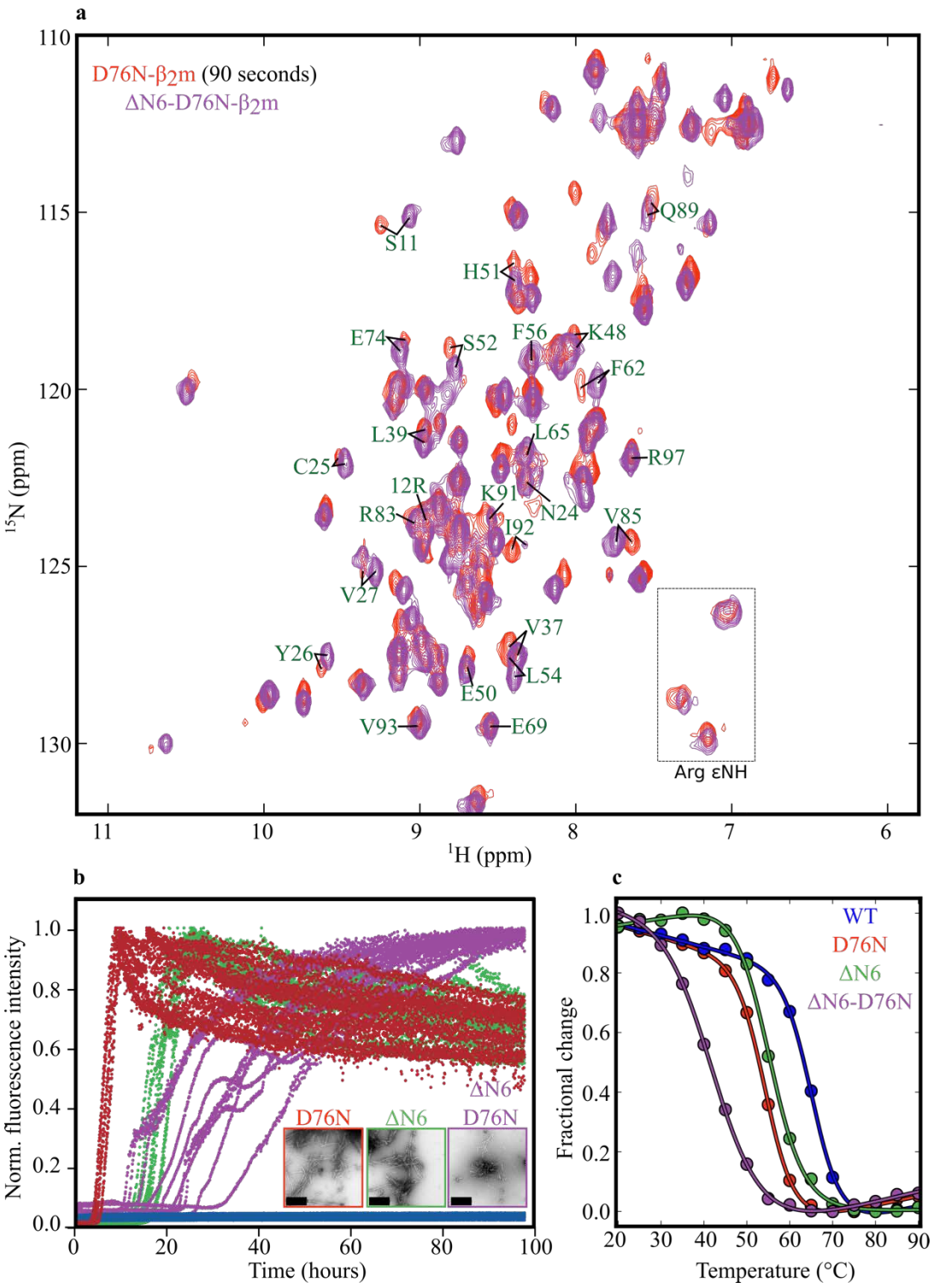

Figure 6. Characterisation of ΔN6-D76N-β_2m.
(a) Superposition of the ^{1}H-^{15}N-SOFAST-HMQC spectra of ΔN6-D76N β_2m (purple) (80 μM protein in 25 mM sodium phosphate pH 7.4, 20 °C) and D76N-β_2m after 90 sec refolding time (red). The 25 peaks unique to the I_T-state are labelled in green. **(b)** Aggregation of ΔN6-D76N- (purple), D76N- (red), ΔN6- (green) and WT-β_2m (blue) (30 μM protein in 25 mM sodium phosphate pH 6.2, 137 mM NaCl, 10 μM

ThT, 0.02 % (*w/v*) NaN_3, 37 °C, 600 rpm). Negative stain transmission EM images of amyloid fibrils from reaction endpoint (taken after 100 h) are shown alongside, framed in the same colours. The scale bar corresponds to 200 nm. Please note that the ThT curves and EM image for D76N-β_2m and WT-β_2m are reproduced from Fig 1b to allow direct comparison with the other proteins shown. **(c)** Stability of different β_2m variants monitored by far-UV CD at 216 nm. The data were fitted using an equation describing a two-state exchange model using the CDPal software package (47) for calculation of $T_{m,app}$ values (Experimental Procedures). The temperature ramp experiment was carried out in 25 mM sodium phosphate pH 6.2, in the range 20-90 °C in 5 °C steps.

Tables and Table Legends

Table 1. Aggregation rates and protein stability of WT-β_2m and the three variants (D76N-, ΔN6- and ΔN6-D76N-β_2m).
Measurements were made in 30 μM protein in 25 mM sodium phosphate pH 6.2, 137 mM NaCl, 10 μM ThT, 0.02 % (*w/v*) NaN_3, 37 °C, 600 rpm for the T_{half}, and 30 μM protein in 25 mM sodium phosphate, pH 6.2 for the $T_{m,app}$. Note that WT-β_2m does not aggregate under the conditions used here over the timespan measured.

Variant	Aggregation T_{half} (h)	$T_{m,app}$ (°C)
WT-β_2m	-	65.5 ± 0.5
D76N-β_2m	6.6 ± 0.7	54.6 ± 0.1
ΔN6-β_2m	18.0 ± 1.9	55.2 ± 0.5
ΔN6-D76N-β_2m	24.7 ± 9.5	42.8 ± 0.9